Chapter 3

Plate-Like Structure Damage Acoustic Emission Beamforming Array Technique and Probability-Based Diagnostic Imaging Method

Dongsheng Li, Mengdao Jin and Quanming Feng

Additional information is available at the end of the chapter

http://dx.doi.org/10.5772/62413

Abstract

A novel beamforming array technique and probability-based diagnostic imaging method are proposed to determine the acoustic emission (AE) source in plate-like structures. The technique that differs from common beamforming array techniques, in particular a sensor network, is used instead of a linear sensor array, to highlight information on the AE source location in one coordinate system as energy distribution. To reduce the uncertainty, avoid the boundary reflection effect, and ensure the rationality of the signal superposition, a Hilbert transform-based signal processing is applied before the delay-and-sum algorithm and a probability-based diagnostic imaging method is developed for AE source localization. The finite element numerical simulation method and the pencil-lead-broken experiment on aluminum plate are also conducted, and a thin-walled cylinder pipe-like structure is also tested by the pencil-lead-broken experiment to develop the application of the proposed method in various fields. The results indicate that this method is efficient and capable of visually showing the localization results highlighted in the probability images.

Keywords: acoustic emission, source localization, beamforming, probability-based diagnosticimaging, plate-like structure, health monitoring

1. Introduction

Plate-like structures are widely used in a variety of fields, such as material, civil, aerospace, and other industries [1–5]. Confirming the health condition of these plate-like structures is a very meaningful assignment for engineers. One of the various non-destructive techniques, acous-

tic emission (AE) monitoring is arguably based on the simplest of physical concepts: the release of transient elastic waves in solid materials as a result of a localized source of damage [2–4]. The process of locating the source of these acoustic waves by capturing the related propagating acoustic signals through various sensors or arrays and properly analyzing them is commonly known as the AE source localization technique [3–8]. Common passive monitoring techniques are currently applied for AE source localization in isotropic and anisotropic structures, particularly in two-dimensional plate-like structures [9,10].

The techniques for AE source localization, such as triangulation technique, modal AE, and optimization-based technique, are currently performed by accurately determining the exact time of arrival (TOA) or time difference of arrival (TDOA) [8]. An obvious disadvantage of these methods is that the precision of the time difference measurement has a great effect on the location precision. To avoid this problem, McLaskey et al. [11] introduced a novel beamforming method of AE analysis, which is particularly suited for field applications on large plate-like reinforced concrete structures, such as walls and bridge decks. The advantage of the beamforming technique is that it does not require the TOA or TDOA of a specific wave mode; the technique can therefore handle noisy signals if the noise is a Gaussian white noise. He et al. [12] applied the beamforming technique for source localization in a thin steel plate through finite element (FE) simulation and experiment. Nakatani et al. [13] studied AE source localization on an anisotropic structure and proved that the technique is simple but effective.

Beamforming has been successfully used in source localization by many researchers, but its limitation as a technique is that it is a velocity-dependent method [11]. As such, its localization accuracy and precision are significantly influenced by the propagation characteristics. The propagation characteristics of an AE signal in plate-like structures are complex because of the signal's repeated reflection in the interface. The wave speed is affected by many factors, such as frequencies, material properties whether isotropic or not, multi-mode, and the dispersion in the propagation process. Xiao et al. [14] proposed a novel beamforming method with two uniform linear arrays in determining the AE source location using an unknown wave speed to reduce the effect of the factors (mentioned earlier) on AE beamforming. However, the accurate two-dimensional position cannot be shown at the same time in one coordinate system, because the localization coordinates are correct along the direction parallel to the array but not along the direction perpendicular to the array.

2. Principle of Lamb wave propagation

The Lamb waves are used to interrogate the whole thickness of the plate-like structures. Either the surface defects or the internal damages can be detected.

2.1. The dispersion characteristic of Lamb wave

Since Lamb waves are waves of plane strain that occur in a free plate, only displacements through the thickness (x_3 direction) and in the direction of wave propagation (x_1 direction) are taken into consideration (**Figure 1**).

http://dx.doi.org/10.5772/62413

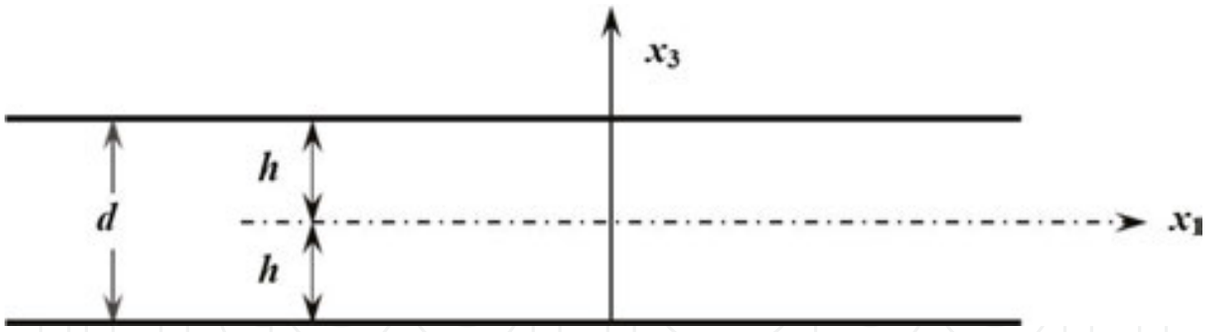

Figure 1. Geometric construction sketching of free plate.

Eq. (1) is for the symmetric Lamb wave mode (S_i, i = 0,1,2,3 ⋯.) in which the particle motion of the plate occurs symmetrically about the symmetric axis of the plate. Eq. (2) is for the anti-symmetric Lamb wave mode (A_i, i = 0,1,2,3 ⋯.) in which the particle motion of the plate occurs asymmetrically about the symmetric axis of the plate [15,16].

$$\frac{\tan(qh)}{\tan(ph)} = -\frac{4k^2pq}{(q^2-k^2)^2}, \tag{1}$$

$$\frac{\tan(qh)}{\tan(ph)} = -\frac{(q^2-k^2)^2}{4k^2pq}, \tag{2}$$

where the parameters p and q are defined as follows:

$$p^2 = \frac{f^2}{c_L^2} - k^2, q^2 = \frac{f^2}{c_T^2} - k^2, h = \frac{d}{2},$$

Where c_L and c_T are the propagation velocities of longitudinal wave and shear wave, respectively; and wavenumber $= \frac{f}{c_P}$.

The phase velocity dispersion curves can be solved by Eqs. (1) and (2). And, the group velocity dispersion curves can be plotted from the phase velocity dispersion curves using Eq. (3). The group velocity and phase velocity dispersion curves for an aluminum plate are shown in **Figure 2**(**a** and **b**).

$$c_g = \frac{c_P^2}{c_P^2 - fd\frac{\partial c_P}{\partial(fd)}}, \tag{3}$$

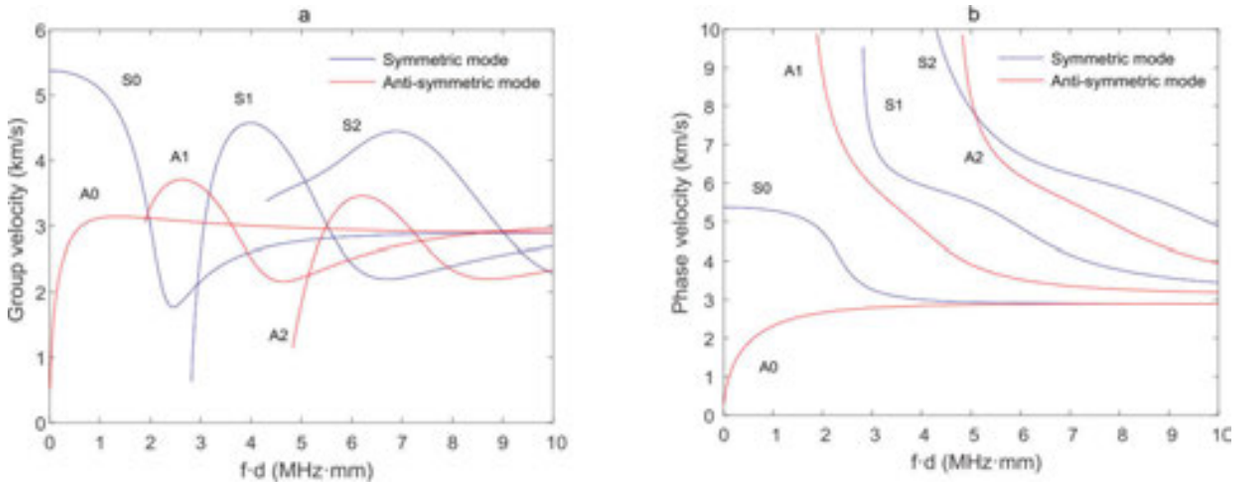

Figure 2. The dispersion curves for an aluminum plate: (a) group velocity dispersion curves and (b) phase velocity dispersion curves.

2.2. Finite element simulation

Numerical simulation is another main method aside from experimental validation that is used in various fields. Modeling the guided waves conveniently provides modeled data with a high signal-to-noise ratio, which can be used to develop useful advanced signal processing and analysis techniques. A number of numerical methods have been applied to analyze the propagation of elastic waves, such as the finite element method (FEM), finite difference method, boundary element method, and finite strip elements (FSE), all of which have their respective merits and defects. FEM is best understood from its practical application, known as finite element analysis (FEA). FEA is a computational tool for performing engineering analysis. It includes the use of mesh generation techniques for dividing a complex problem into small elements, which in turn represent different areas in the physical system; the technique also uses a software program coded with the FEM algorithm. This study simulates the guided wave signal propagation with FEA in the general three-dimensional domain using the commercial package ABAQUS, which has some advantages and is effective. It easily records the solution results of every element or node by time step and extracts results. In addition, it provides sophisticated pre- and post-processing functions and is user-friendly. Many scholars have demonstrated the possibility of using FEM to solve the guided wave formation and guided wave signal propagation in plate specimens.

2.2.1. Explicit dynamic analysis

The explicit dynamics analysis procedure, ABAQUS/Explicit, is based upon the implementation of an explicit integration rule together with the use of diagonal ("lumped") element mass matrices. The equations of motion for the body are integrated using the explicit central-difference integration rule.

http://dx.doi.org/10.5772/62413

$$\dot{u}_{\left(i+\frac{1}{2}\right)} = \dot{u}_{\left(i-\frac{1}{2}\right)} + \frac{\Delta t_{(i+1)} + \Delta t_{(i)}}{2} \ddot{u}_{(i)}, \tag{4}$$

$$u_{(i+1)} = u_{(i)} + \Delta t_{(i+1)} \dot{u}_{\left(i+\frac{1}{2}\right)}, \tag{5}$$

Where u is a degree of freedom (a displacement or rotation component) and the subscript i refers to the increment number in an explicit dynamics step.

The explicit procedure integrates through time by using many small time increments. The central-difference operator is conditionally stable, in order to avoid numerical instability, there are more than 20 points per cycle of the highest frequency. Therefore, the time step can be expressed as follows [17]:

$$\Delta t = \frac{1}{20 f_{max}}, \tag{6}$$

where f_{max} is the highest frequency of interest.

The size of the finite element is depended on the smallest wavelength. In reference [17], it is recommended that 20 nodes per wavelength be used. So that, it can be expressed as

$$l_e = \frac{\lambda_{min}}{20}, \tag{7}$$

where l_e is the element size and λ_{min} is the shortest wavelength of interest.

In the present FEM analysis,Δ t = 0.1 μs and l_e = 1 mm. The plate was discretized using brick elements C3D8R, and the mesh is shown in **Figure 3**. The physical properties of the aluminum plate areas follows: E = 71 GPa, ν = 0.33, ρ = 2700 kg/m^3.

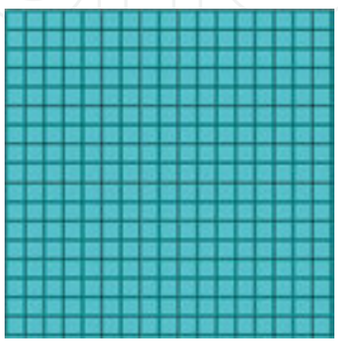

Figure 3. The structured meshing technique.

2.2.2. Excitation signal

In the finite element modeling, the excitation signal is a smoothed tone burst obtained by filtering a five-cycle pure tone burst of central frequency f = 150 kHz through a Hanning window [**Figure 4**(**a** and **b**)].The Hanning window is described by the following equation [18]:

$$h(t) = 0.5 \cdot \left[1 - cos\left(\frac{2\pi t}{T}\right)\right], \quad t \in [0, T] \tag{8}$$

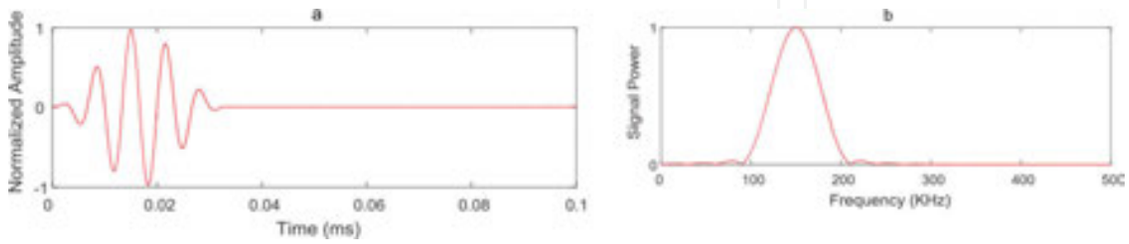

Figure 4. Five-cycle Hanning window-modulated sinusoid tone bursts in: (a) time domain and (b) frequency domain after Fast Fourier Transform.

The number of counts *(N)* in the tone bursts matches the length of the Hanning window:

$$T = \frac{N}{f} \tag{9}$$

The smoothed tone burst is governed by the following equation:

$$x(t) = h(t) \cdot sin(2\pi ft), \quad t \in [0, T] \tag{10}$$

2.2.3. Selective excitation of Lamb wave modes

Dual piezoelectric (PZT) actuators are symmetrically mounted on the top and bottom surfaces of a plate, and the frequencies of excitation signals are controlled to a range so as to generate the fundamental symmetric mode S_0 and anti-symmetric mode A_0 only. This mode selection technique can be expressed as:

1. When either of the dual PZTs is energized, both the symmetric mode S_0 and the anti-symmetric mode A_0 will be generated simultaneously.
2. When dual PZTs are in-phase energized, the symmetric mode S_0 with the most signal energy is generated, meanwhile, the anti-symmetric mode A_0 is weaker.
3. When dual PZTs are out-phase energized, the anti-symmetric mode A_0 is generated to dominate the majority of wave energy, and the symmetric mode S_0 is suppressed.

http://dx.doi.org/10.5772/62413

In the FEM, a 1200 mm × 1200 mm aluminum plate with 4 mm thickness was used for the simulation. Because the piezoelectric element C3D8E doesn't exist in ABAQUS/explicit; so we applied 16 self-equilibrating concentrated forces, as shown in **Figure 5**., to simulate the wave excitation for the round PZT actuators. The mode excitation method is expressed as follows:

When the 16 self-equilibrating concentrated forces are loaded on the top or the bottom of a plate, both S_0 mode and A_0 mode are excited simultaneously.

When the 16 self-equilibrating concentrated forces are symmetrically loaded on the top and the bottom of a plate, the mode S_0 will be excited.

When the 16 self-equilibrating concentrated forces are anti-symmetrically loaded on the top and the bottom of a plate, the mode A_0 will be excited. The excited Lamb wave modes are shown in **Figure 6**(**a**–**c**).

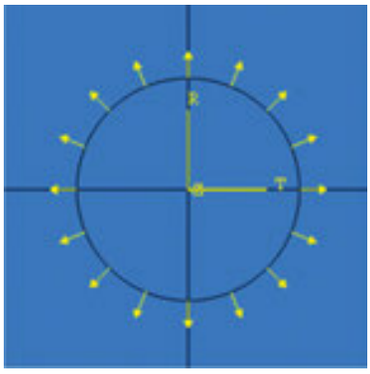

Figure 5. Self-equilibrating concentrated forces for round PZT actuators.

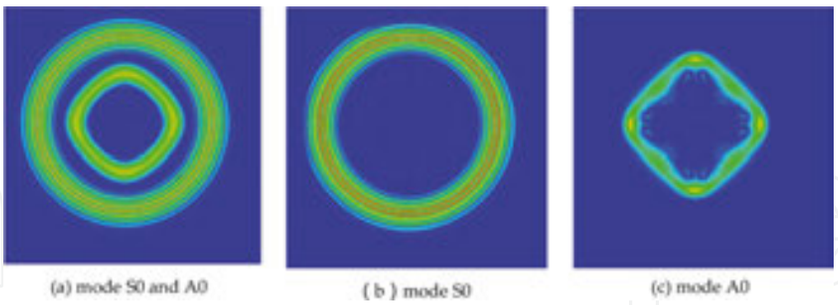

Figure 6. The excited Lamb wave modes.

2.2.4. Lamb wave scattering simulations

2.2.4.1. The interaction of the S_0 mode with a circular hole

It is well known that mode conversion phenomena will occur when the incident S_0 mode wave interacts with damages; there will be S_0 mode, A_0 mode, and SH0 mode waves in the scattering fields.

When the depth of the hole is through thickness, the scattering S_0 mode and SH0 mode can be captured.

When the depth is 75% of the thickness, the scattering S_0 mode, A_0 mode, and SH0 mode can be captured.

The snapshots of S_0 mode interaction with a circular hole are shown in **Figure 7** and **Figure 8**, respectively.

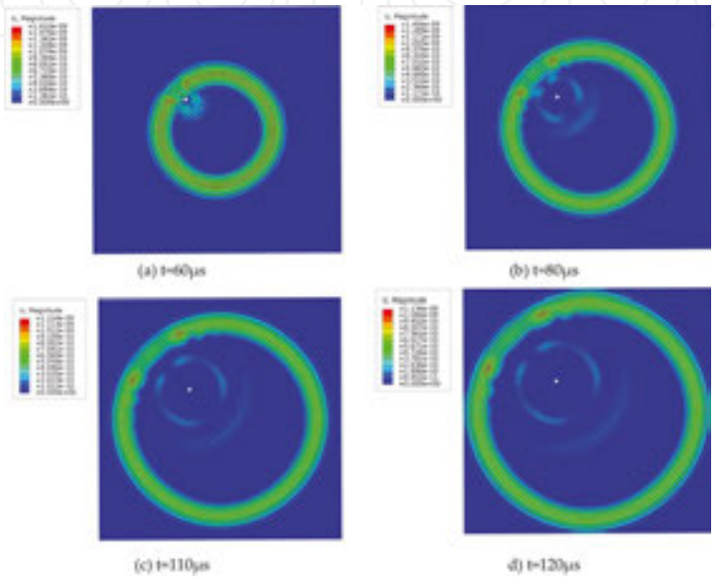

Figure 7. The scattering field of a through-thickness hole.

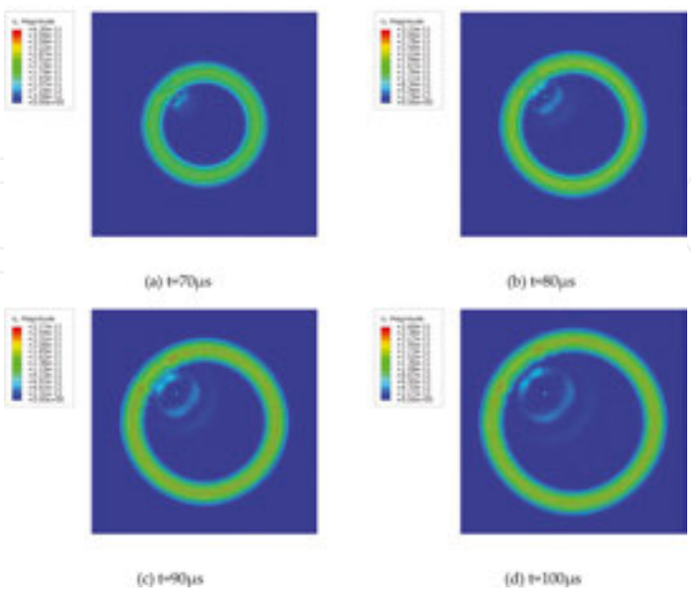

Figure 8. The scattering field of a hole with the depth is 75% of the thickness.

http://dx.doi.org/10.5772/62413

2.2.4.2. The interaction of the S_0 mode with a crack

When the incident S_0 mode wave interacts with a crack, the crack-induced scattering wave components are same as a circular hole. The snapshots of S_0 mode interaction with a crack are shown in **Figure 9**.

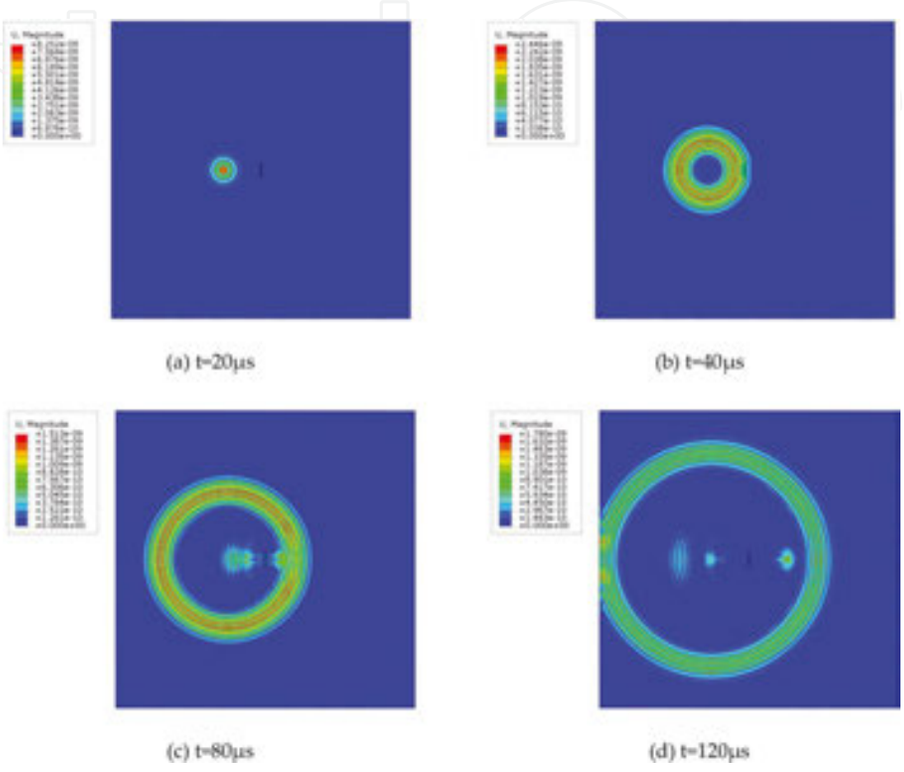

Figure 9. The scattering field of a through-thickness crack.

3. Beamforming algorithm for damage identification

3.1. Principle of the beamforming network method

The beamforming technique is a method based on the delay-and-sum algorithm. **Figure 10** shows that an acoustic event causes an AE source to generate an acoustic wave, which is received by M sensors. Given the difference between the distance of the sensors and that of the sound source, the arrival time must also differ. Although different degrees of attenuation exist on the wave energy, waveform parameters, such as frequency, duration, and the peak of the same sound source remain almost same. The beamforming technique adjusts different sensor waveform signals to the same datum point by time delay to ensure that the entire waveform signal is adjusted to the same wave front. The sensors network output of incident waves in an isotropic plate is expressed by Eq. (11). The variable $b(\vec{r}, t)$ is the network output with the delay-and-sum algorithm, after applying time delays $\Delta_m(\vec{r})$ to the recorded signals

and multiplying them with the weight factor as shown further. According to **Figure 1**, the $\Delta_m(\vec{r})$ can be obtained by Eq. (12).

$$b(\vec{r},t)=\frac{1}{M}\Sigma_{m=1}^{M}w_m x_m(t-\Delta_m(\vec{r}))\,, \tag{11}$$

$$\Delta_m(\vec{r})=\frac{|\vec{r}|-|\vec{r}-\vec{r}_m|}{c}\,, \tag{12}$$

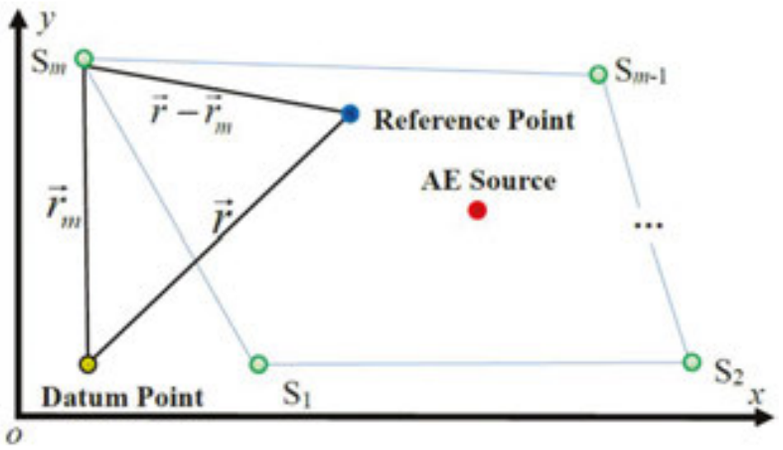

Figure 10. Principle illustration of the beamforming network method.

Here the variable $x_m(t)$ represents the measured signal acquired by the m_{th} (m = 1, 2,…, M) sensor S_m. $\vec{r}$ represents the distance of a reference point (also called the focal point) from the previously designated datum point, and $\vec{r}_m$ represents the distance of a reference point from the m_{th} sensor. $\Delta_m(\vec{r})$ is the individual time delay for the m_{th} sensor, and c is the propagation velocity of the acoustic wave. Different reference points (or focal points) have different time delays $\Delta_m(\vec{r})$. By adjusting time delays $\Delta_m(\vec{r})$, the signals associated with the spherical waves emitted from the sound source focus are aligned in time before they are summed. When the reference point and the acoustic source point coincide, the signals are aligned at the same wave front, and the energy output of the sensor network is at its maximum. Beamforming technology compares the network output results of each reference point and displays them into the position-energy curve after normalized processing. The position of the maximal energy distribution is the location of the sound source, and all the weight factors w_m may be taken as 1.

3.2. Hilbert transform-based signal processing

Given the propagation of the elastic wave in materials, the reflection and scattering of signals result in mode conversion, which goes against waveform processing. Research findings have

http://dx.doi.org/10.5772/62413

shown that an energy distribution curve with pure signal superposition is not continuous, as shown in **Figure 11(a)**. Beamforming technology needs only the necessary amplitude information and does not require the full waveform information. Thus, to reduce the uncertainty, avoid the boundary reflection effect, ensure the rationality of the superposition, and obtain a smooth curve, the envelopes of the signals obtained using Hilbert transform (HT)-based signal processing $A_m(t)$ (i.e., the first wave packet containing the peak information is intercepted) are used in this study instead of the signal variable $x_m(t)$. The parameter B given in Eq. (15) attains the maximum value when the reference point coincides with the AE source point. The HT series given in Eqs. (13) and (14) have the same amplitude and frequency content as the original data and include phase information, which depends on the phase of the original data, as shown in **Figure 11(b)**. The same source results demonstrate that the HT-based signal processing $A_m(t)$ is reasonable and capable of obtaining the energy distribution information of the AE source, as shown in **Figure 11(c)**.

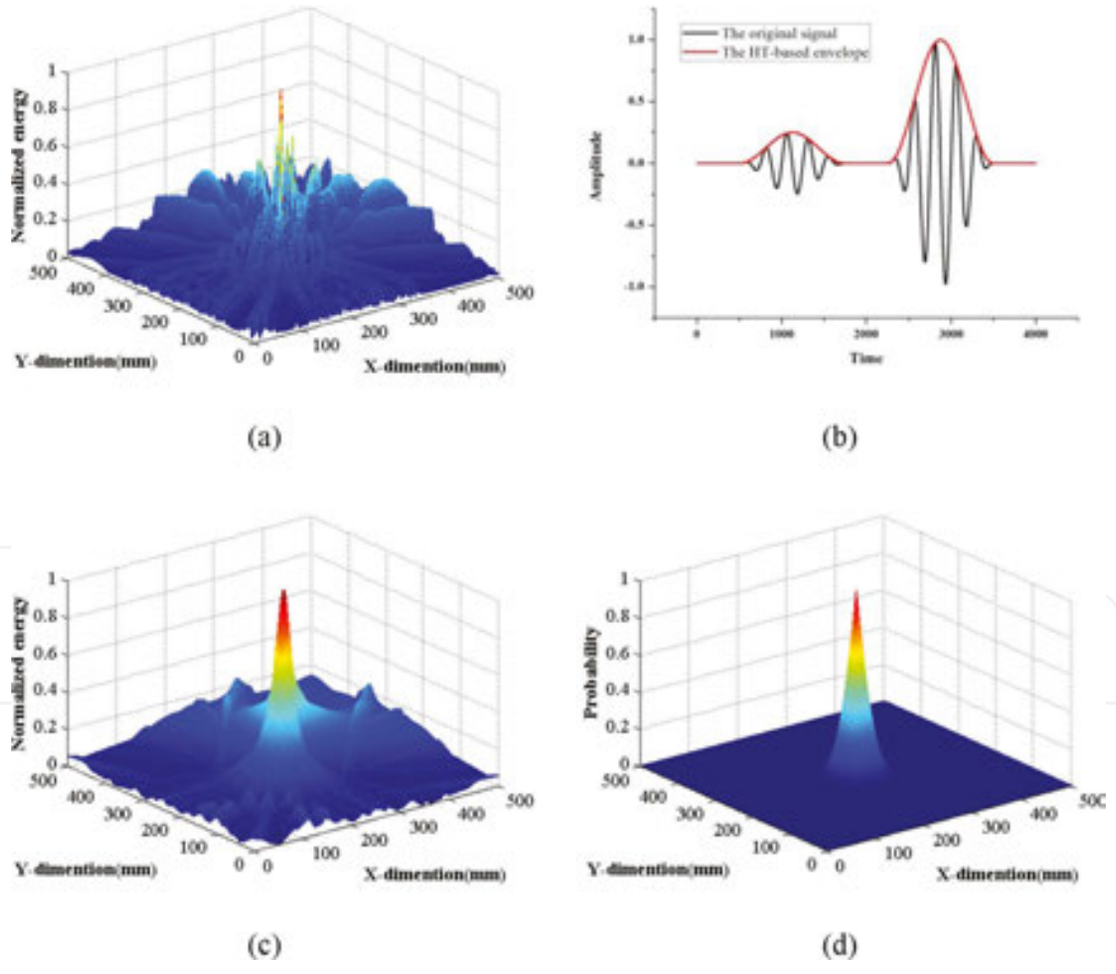

Figure 11. Localization results in multiple ways. (a) The normalized energy distribution with original signals $x_m(t)$; (b) the original signals and the HT-based envelopes; (c) the normalized energy distribution with HT-based envelopes $A_m(t)$; and (d) the probability distribution.

$$\hat{x}_m(t) = \int_{-\infty}^{+\infty} \frac{x_m(\tau)}{\pi(t-\tau)} d\tau \ , \tag{13}$$

$$A_m(t) = \sqrt{x_m^2(t) + \hat{x}_m^2(t)} \ , \tag{14}$$

$$B(\vec{r},t) = \frac{1}{M} \Sigma_{m=1}^{M} w_m A_m(t - \Delta_m(\vec{r})) \ , \tag{15}$$

3.3. Probability-based diagnostic imaging

Given the existence of errors and uncertainty, the real location of the sound source is likely to be where the energy is larger (near the maximum). Thus, a probability diagnostic imaging technology is introduced to explain the results from the perspective of probability theory. After determining the energy distribution, the structure under detection is meshed using L × K nodes for probability-based diagnostic imaging; this technique is an emerging technique for monitoring the health status of a structure and identifying damages and has attracted much attention in recent years [19, 20]. It uses an easily interpretable image whose pixels exclusively correspond to the spatial points to describe the health status of the structure. The field value of a pixel stands for the probability of the presence of damage at the point of the structure corresponding to the pixel, and the degree of probability is often calibrated through different gray scales. In this study, the normalized energy distribution can be regarded as the probability of the AE source location. When the normalized energy distribution focuses on a peak under the correct circumstances, it is similar to the Gaussian distribution. Thus, a cumulative distribution function, $F(z)$, is introduced to facilitate this procedure of defining the field value asfollows:

$$F(z) = \int_{-\infty}^{z} f(z) dz \ , \tag{16}$$

$$f(z) = \frac{1}{\sigma\sqrt{2\pi}} exp\left(-\frac{z^2}{2\sigma^2}\right), \tag{17}$$

$$z = \sqrt{(x_i - x_p)^2 + (y_i + y_p)^2} \ , \tag{18}$$

where $f(z)$ is the Gaussian distribution function, which represents the probability density of the presence of the AE source at the mesh node $(x_i, y_j)(I = 1, 2, \ldots, L; j = 1, 2, \ldots, K)$. The variable z is the distance of the arbitrary node (x_i, y_j) to the node (x_p, y_p), whose peak point is in the normalized energy distribution, and σ is the standard variance. Thus, the field value at node (x_i, y_j), which is the probability of the AE source $I(x_i, y_j)$ is

http://dx.doi.org/10.5772/62413

$$I\left(x_i, y_j\right) = 1 - \left[F(z) - F(-z)\right], \tag{19}$$

The normalized energy and probability distributions of AE localization results are shown in **Figure 11(d)**.

4. FE model of AE simulation

A sketch of the FE model with the geometric configuration 800 mm × 600 mm × 4 mm is shown in **Figure 12**. The homogeneous isotropic aluminum plate is characterized by the following: Young's modulus E = 71 GPa, Poisson ratio v = 0.33, and mass density ρ = 2700 Kg/m^3. In this model, damping is not considered, the boundaries are free, and a total of eight sensors (S1–S8) form a rectangular network. The AE source position, datum point, and their location are marked, and the three AE sources are named as cases A, B, and C. All the cases are considered both away from and close to the boundary. All of the sensors are decorated (geometrically) evenly. A Hanning-windowed five-cycle sinusoidal tone burst is used as the transient excitation to simulate the AE wave. The frequency of the excitation signal is 400 KHz. A same off-plane displacement with a peak of 0.1 μ m is loaded on multiple cases, and the time histories of the samples of the sensor nodes are captured. The element size and integration time step in FEA process are designated as 2 mm and 0.1 μs, respectively, to avoid numerical instability [19].

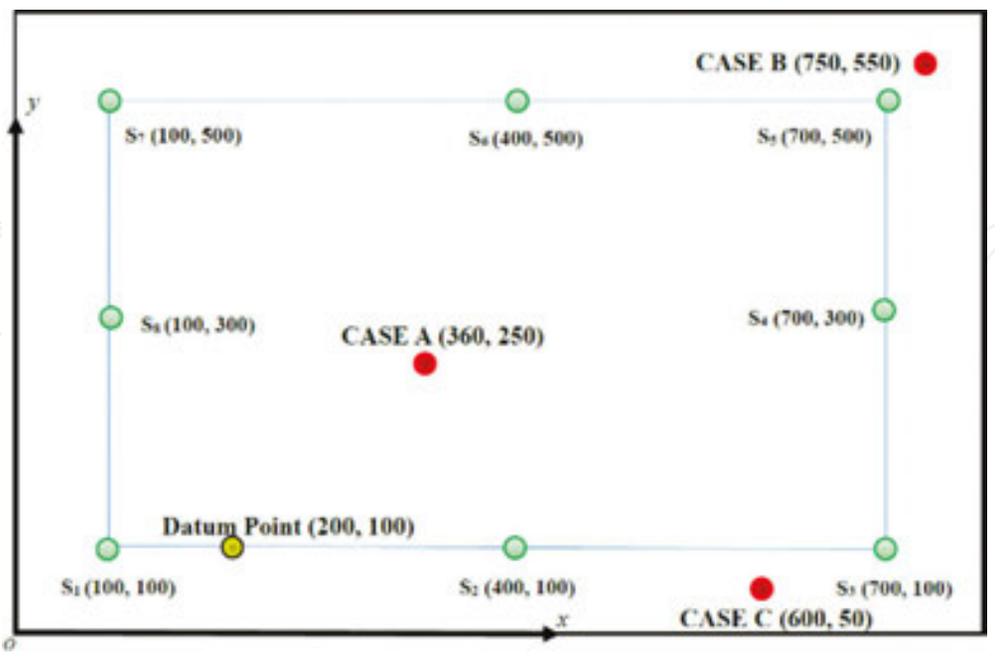

Figure 12. Setup of FE model of AE simulation configuration with a rectangular network.

The AE wave is a common form of the Lamb wave propagation in plate-like structures. In most cases, multiple Lamb modes exist simultaneously, and the dispersive properties of such modes are not identical even for the same mode in different frequency ranges [21]. Different mode waves travel with different groups and phase velocities. As a consequence, source localization strategies must be conducted based on a certain wave propagation mode. The fundamental symmetric mode S_0 wave and the fundamental asymmetric mode A_0 wave are popularly used in plate-like structures. The localization results are presented using S_0 mode wave, given that the propagation velocity of the S_0 mode is faster than that of the A_0 mode and considering the interception of the first wave packet analyzed in this study. The dispersion curve in **Figure 13** shows that the propagation speed of the S_0 mode Lamb wave with a frequency of 400 KHz in 4 mm unconstrained aluminum plate is about 4600 m/s.

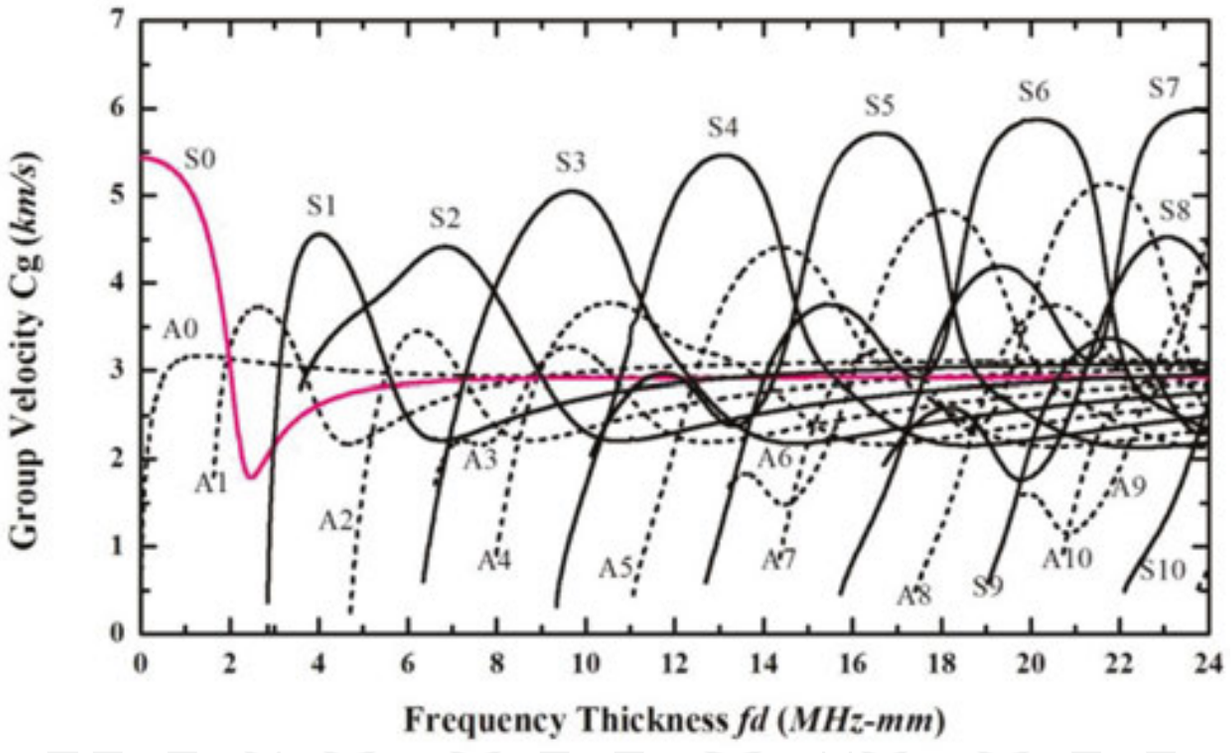

Figure 13. Dispersion curves of Lamb wave in the free isotropic aluminum plate.

4.1. Localization results of the numerical simulation

To verify the validity of the positioning, three cases of real sound sources were tested using the delay-and-sum algorithm with the precise wave speed. Their real coordinates were as follows: case A (360 mm, 250 mm), case B (750 mm, 550 mm), and case C (600 mm, 50 mm). The localization results for the rectangular sensor network are exhibited in **Table 1**.

http://dx.doi.org/10.5772/62413

Multiple case	Normalized energy distribution with HT	Probability distribution
Case A	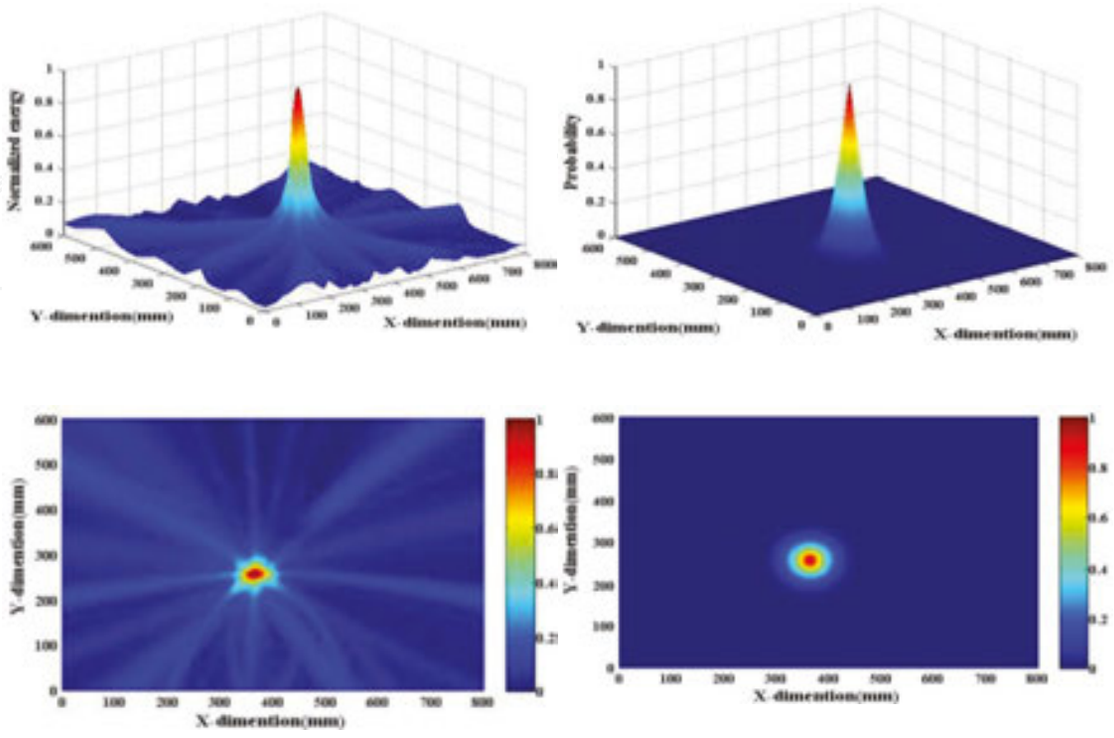	
Case B	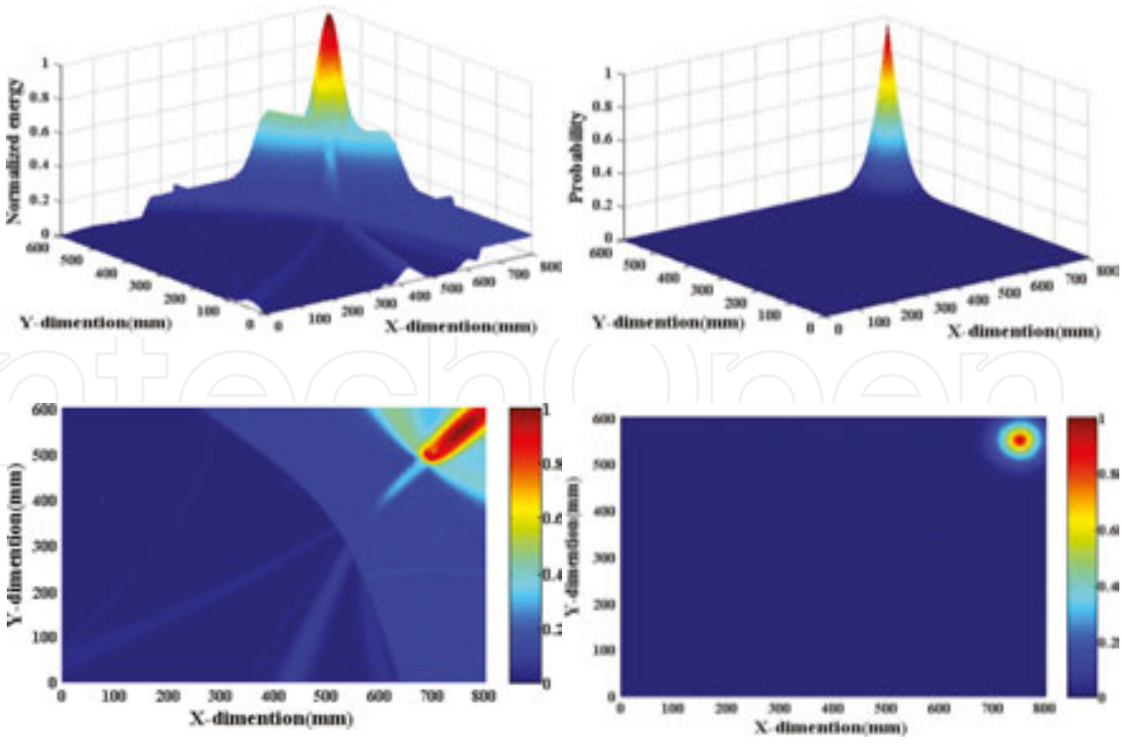	

Multiple case	Normalized energy distribution with HT	Probability distribution
Case C	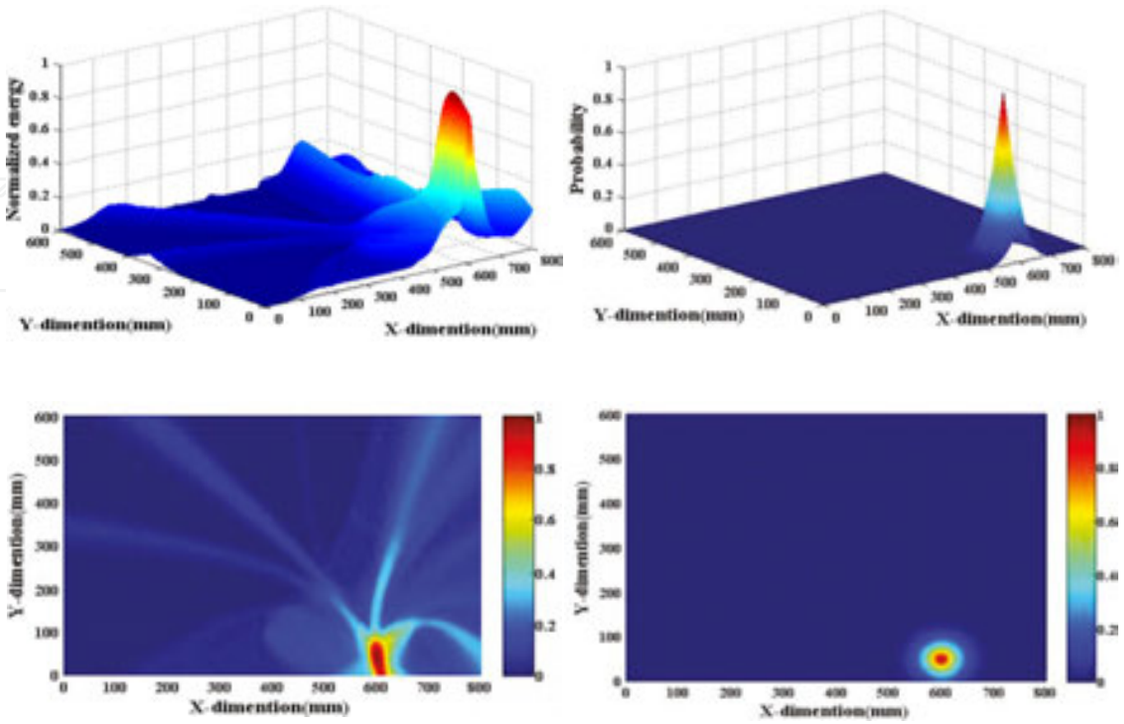	

Table 1. Multiple cases of the source localization for aluminum plate based on beamforming method with rectangular sensor network in wave velocity c = 4600 m/s

The results show that under the true known wave speed, the beamforming array technique and probability-based diagnostic imaging method can confirm the location of the AE source and produce accurate positioning results, as highlighted in the floor plan image. The case away from boundaries can evidently work much better than the cases close to boundaries, given the same wave speed. The results also prove that HT-based signal processing and probability-based diagnostic imaging are reasonable and effective.

4.2. The influence of the wave speed

The localization results in **Table 1** show that the beamforming technique can effectively confirm the location of the AE source and produce accurate positioning results, as highlighted in the floor plan image. However, it is a wave-velocity-dependent method; a clear limiting factor of this technique is the need to obtain knowledge on its wave propagation speed. For common, uniform, and thick plate materials, we generally find out the dispersion curve to determine the required wave velocity, following the theory of wave propagation. However, given the structure size, material properties, or performance degradation factors, ensuring the dispersive curves of the Lamb wave is not easy, so the sound source localization of the plate structure in the case of unknown wave velocity must be discussed.

http://dx.doi.org/10.5772/62413

According to beamforming theory, the largest impact of wave velocity lies on the length of delay. Under a real wave velocity, signals can be achieved through accurate time delay adjustment to the same wave front, the superposition of energy concentrated, and the maximum output reached. In calculating a wave velocity that is far from the true wave velocity, the energy is unable to concentrate and the peak isn't the maximum. This finding can be proven by **Figure 14**.

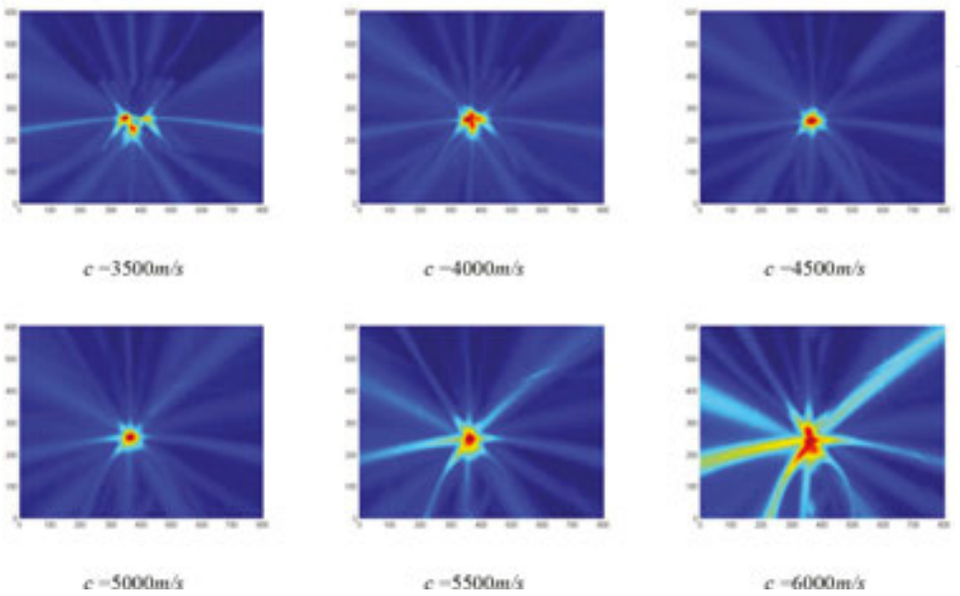

Figure 14. The localization results of case A under different wave speed.

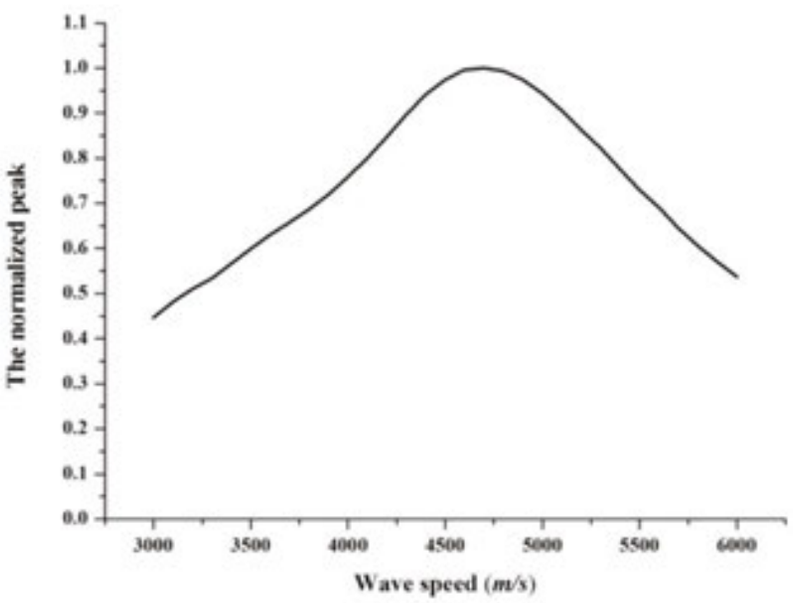

Figure 15. The normalized energy peak curves of FE model in different wave speeds.

The larger the deviation from the real wave velocity, the higher the divergence of the energy; the smaller the deviation from the real wave velocity, the more concentrated the stack power. The normalized energy peak curves of the FE model under different wave speeds are shown in **Figure 15**. When the wave speed is 4700 m/s, the peak of the energy is at its maximum, so that the real wave velocity is around 4700 m/s. At this rate, the localization can also be confirmed by comparing the energy distribution or peak value under the different wave speeds, with no need for the known real wave velocity.

5. Experimental verification

To further verify the effectiveness of AE source localization using beamforming network technology for plate-like structures, a pencil-lead-broken experiment on an aluminum plate and a steel cylinder experiment are implemented.

5.1. Aluminum plate experiment

The size of the aluminum plate adopted in the experiment was 1000 mm × 1000 mm × 4 mm. It was a homogeneous isotropic aluminum plate with the following characteristics: Young's modulus E = 71 GPa, Poisson ratio v = 0.33, and mass density ρ = 2700 Kg/m^3. A rectangular network with eight AE sensors was built, with each of the sensors placed 100 mm away from the closed boundary. An AE acquisition system from Physical Acoustics Corporation was applied in the experiment, and the sampling frequency used was 1 M/s. The pencil-lead-broken experiment was used to simulate the AE source (**Figure 16**). Multiple cases of the source location were set in Cases A (500 mm, 500 mm), B (200 mm, 500 mm), and C (700 mm, 300 mm).

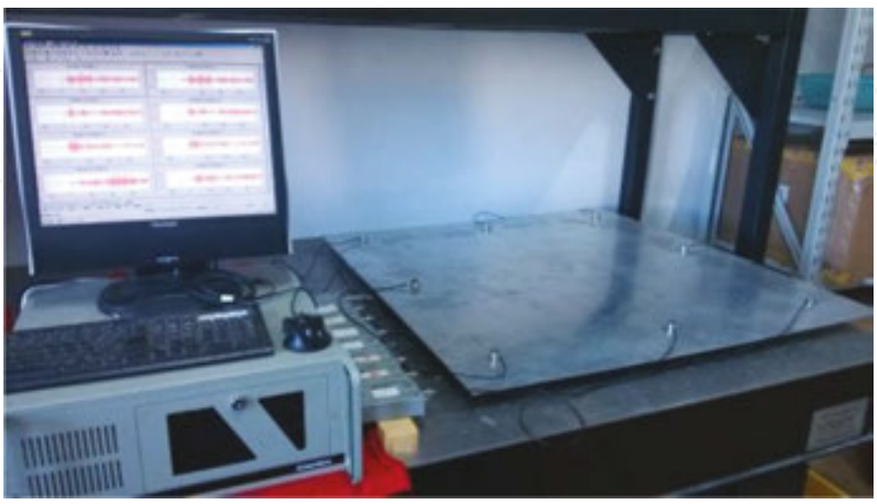

Figure 16. Aluminum plate experiment system.

http://dx.doi.org/10.5772/62413

According to the chapter 3. 1 mentioned method, the normalized energy peak curves of experimental aluminum plate under different wave speeds were shown in **Figure 17**. The AE propagation speed was about 5200 m/s. The localization results for the rectangular sensor network are exhibited in **Table 2**.

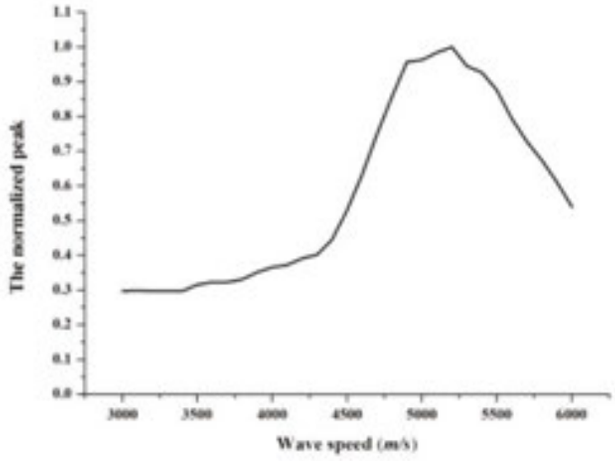

Figure 17. The normalized energy peak curves of 4 mm aluminum plate.

Multiple case	Normalized energy distribution with HT	Probability distribution
Case A	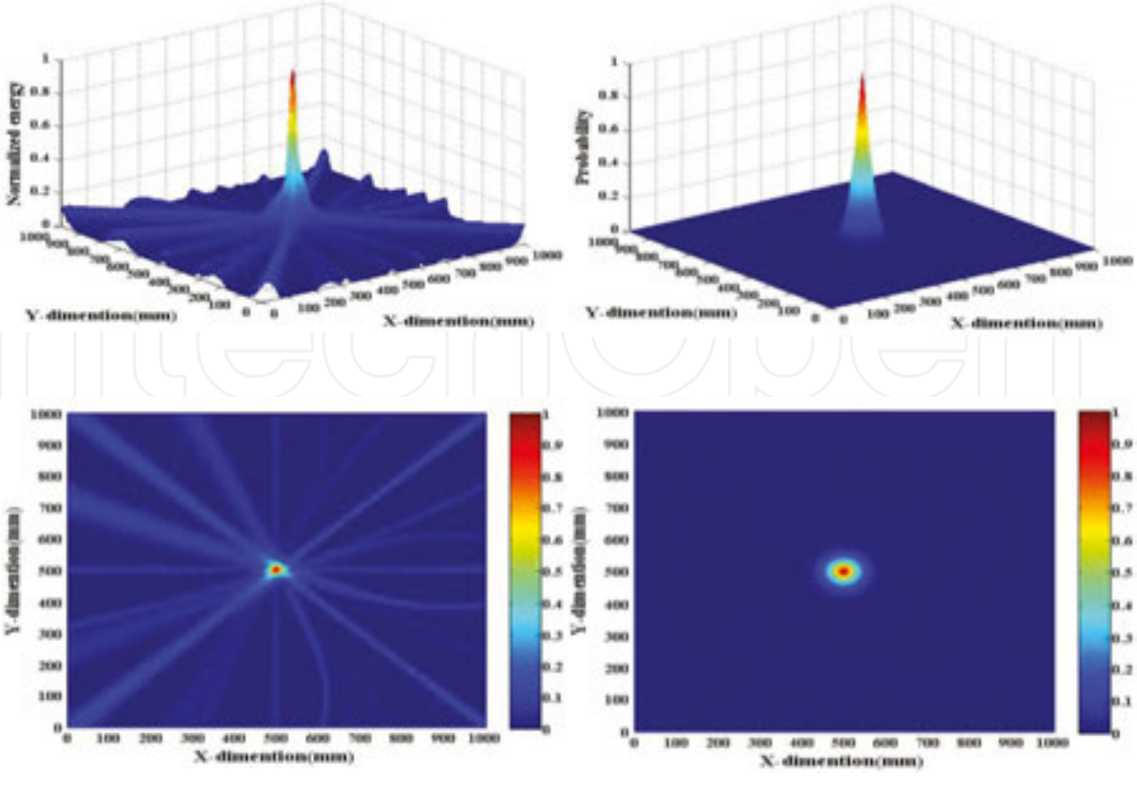	

Multiple case	Normalized energy distribution with HT	Probability distribution
Case B	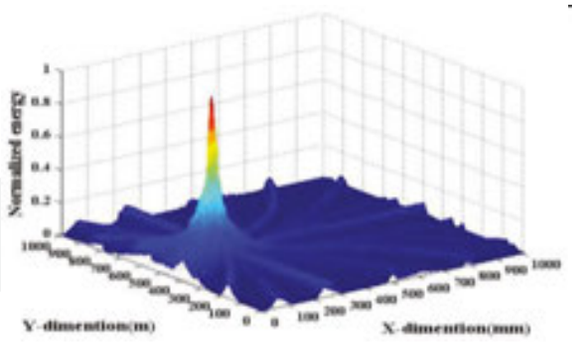	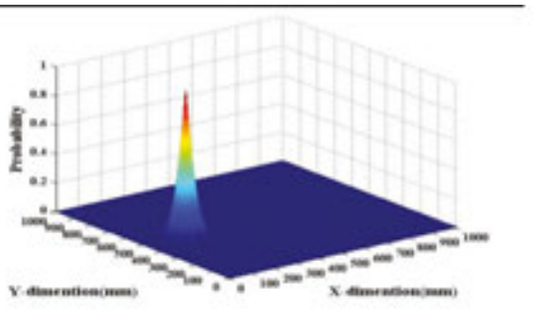
	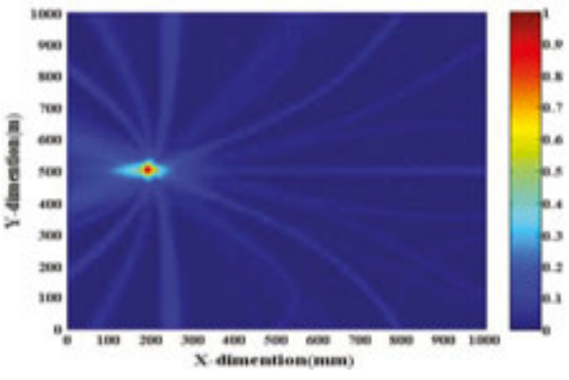	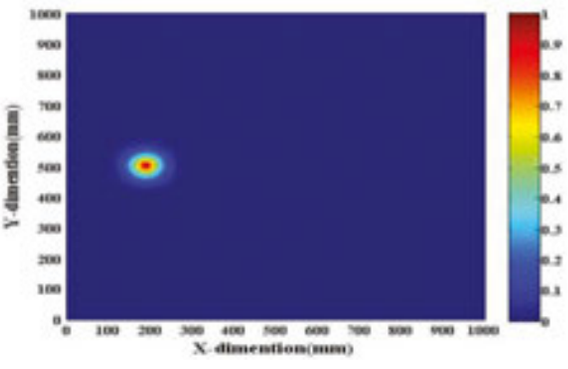
Case C	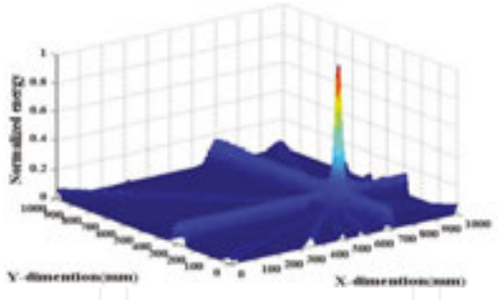	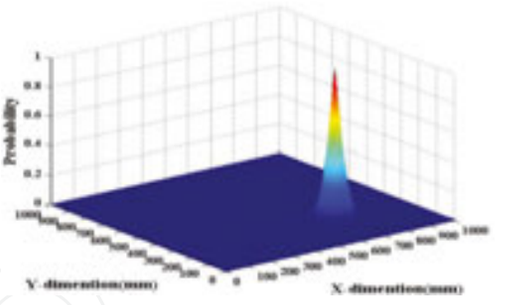
	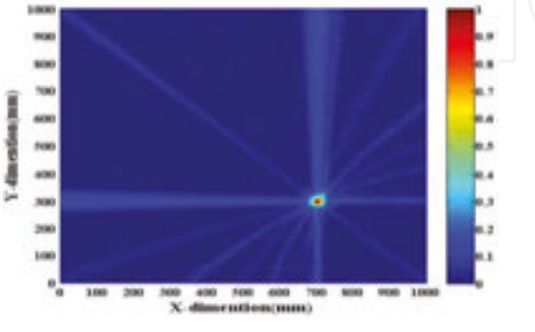	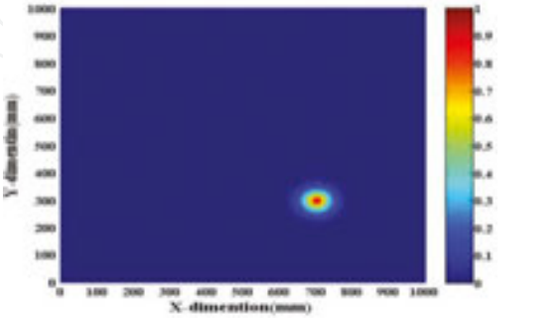

Table 2. Multiple cases of the source localization for aluminum plate based on beamforming method with rectangular sensor network in wave velocity c =5200m/s

http://dx.doi.org/10.5772/62413

5.2. Thin-walled steel cylinder experiment

For a thin-walled cylinder with a large radius, the propagation characteristics of the Lamb wave are the same as those of plate-like structure [22]. Thus, this study constructed a sensor network in conformity to a plate on a steel thin-walled cylinder to verify the effectiveness of the beamforming method for AE source localization. The cylinder had an inner radius, external radius, and height of 102, 110, and 700 mm, respectively, and was characterized by the following: Young's modulus E = 209 GPa, Poisson ratio v = 0.3, and mass density ρ = 7800 Kg/m^3. The sensors were arranged, such that the circles with the heights of 100 and 600 mm were stepped by 90° (**Figure 18**). The chosen generatrix was 0°, and the X-axis was transformed into a degree measure. The AE source position was designed at (90°, 350 mm); according to the normalized energy peak curves of the 8 mm steel cylinder in **Figure 19**, the wave velocity was 4900 m/s. Given the strong symmetry of the cylinder, some of the sensors could be used more than once, so that beamforming network algorithm was achieved at a step of 90°. The localization result and energy and probability distribution are exhibited in **Table 3**. It was verified that the algorithm can be applied to AE source localization for thin-walled steel cylinders.

Figure 18. Thin-walled cylinder pipe-like structure experimental system.

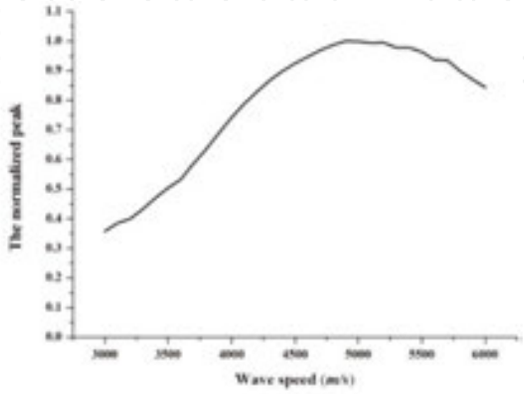

Figure 19. The normalized energy peak curves of 8 mm steel cylinder with different wave speeds.

Normalized energy distribution	Probability distribution
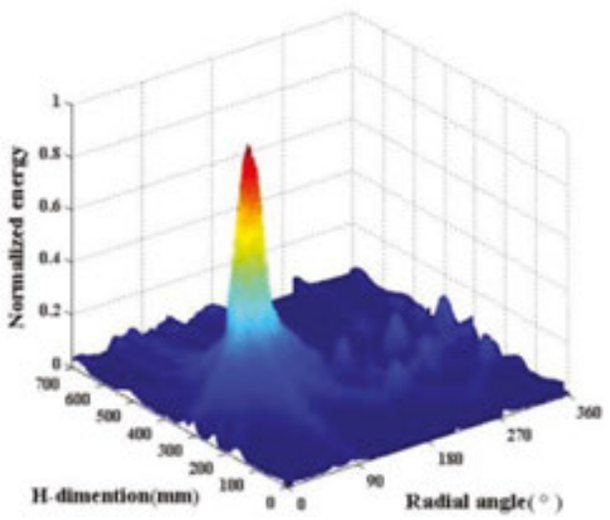	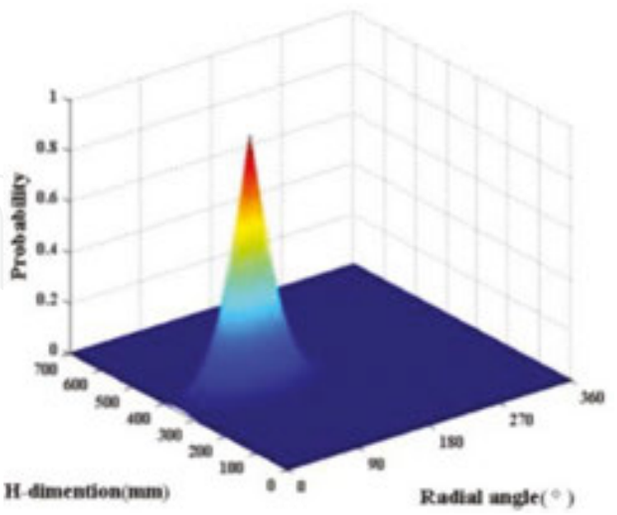
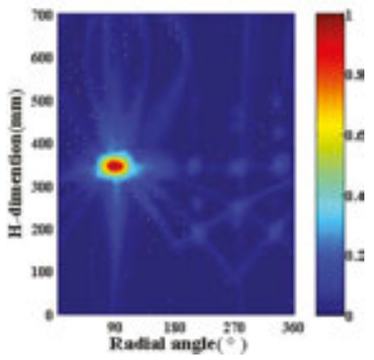	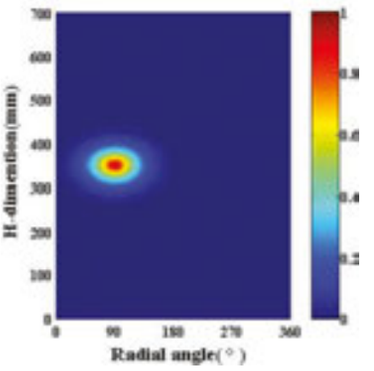

Table 3. The AE source localization for thin-walled steel cylinder based on beamforming method with rectangular sensor network in wave velocity c = 4900 m/s.

6. Conclusion

This study investigates AE source localization in plate-like structures using the beamforming network method and probability-based diagnostic imaging. Some conclusions based on the analysis of the localization results are drawn below.

(1) The beamforming technique is effective for AE source localization without the TOA or TDOA. Unlike other localization techniques, it is simple because it avoids the acquirement of detailed information on signals. Through the beamforming network algorithm, the AE source location information is highlighted in one coordinate system as energy distribution.

(2) An HT-based signal processing method was developed. The testing results demonstrate that the HT-based signal processing method is reasonable and capable of obtaining the energy

http://dx.doi.org/10.5772/62413

distribution information of the AE source. Moreover, a probability diagnostic imaging technology is introduced to improve localization accuracy. The field value of a pixel stands for the probability of the presence of damage at the point of the structure corresponding to the pixel, and the degree of probability is often calibrated through different gray scales.

(3) When the wave speed is known, the beamforming technique can accurately determine the source localization, no matter how far away from or close it is to the boundaries of the structure. Even if the wave velocity is unknown, the localization can also be confirmed by comparing the energy distribution or peak values under different wave speeds, as proven accurately in this study.

(4) The algorithm can also be applied to AE source localization in thin-walled steel cylinders pipe-like structure. However, its applicability in long axial length structures is yet to be verified.

Acknowledgements

The authors are grateful for the financial support from National Natural Science Foundation of China (NSFC) under Grant numbers 51278083, 51478079, and Science and Technology Project of Fujian Province (Grant number 2012Y01010047).

Author details

Dongsheng Li*, Mengdao Jin and Quanming Feng

*Address all correspondence to: lidongsheng@dlut.edu.cn

School of Civil Engineering, Dalian University of Technology, China

References

[1] A. Peter, A. Fehervary. Evaluation of acoustic emission from pressure vessels with planar. Theoretical and Applied Fracture Mechanics. 1986;5:17–22.

[2] P. Pellionisz, P. Szüc. Acoustic emission monitoring of pressure vessels. International Journal of Pressure Vessels and Piping.1993;55:287–294.

[3] D. Aljets, A. Chong, S. Wilcox, K. Holford. Acoustic emission source location on large plate-like structures using a local triangular sensor array. Mechanical Systems and Signal Processing. 2012;30:91–102.

[4] T. Kundu, H. Nakatani, N. Takeda. Acoustic source localization in anisotropic plates. Ultrasonics. 2012;52:740–746.

[5] A. Tobias. Acoustic emission source location in two dimensions by an array of three sensors. Nondestructive Testing. 1976;9:9–12.

[6] B. Castagnede, W. Sachse, K.Y. Kim. Location of point like acoustic emission sources in anisotropic plates. Journal of the Acoustical Society of America. 1989;86:1161–1171.

[7] T. Kundu, S. Das, S.A. Martin, K.V. Jata. Locating point of impact in anisotropic fiber reinforced composite plates. Ultrasonics. 2008;48(3):193–201.

[8] T. Kundu. Acoustic source localization. Ultrasonics. 2014;54:25–38.

[9] Archana Nair, C.S. Cai. Acoustic emission monitoring of bridges: review and case studies. Engineering Structures. 2010;32(6):1704–1714.

[10] Marwa Abdelrahman, Mohamed K. ElBatanouny, Paul H. Ziehl. Acoustic emission based damage assessment method for prestressed concrete structures: modified index of damage. Engineering Structures. 2014;60: 258–264.

[11] G.C. McLaskey, S.D. Glaser, C.U. Grosse. Beamforming array techniques for acoustic emission monitoring of large concrete structures. Journal of Sound and Vibration. 2010;329(12):2384–2394.

[12] T. He, Q. Pan, Y. Liu, X. Liu, D. Hu. Near-field beamforming analysis for acoustic emission source localization. Ultrasonics. 2012;52(5):587–592.

[13] H. Nakatani, T. Hajzargarbashi, K. Ito, et al. Locating point of impact on an anisotropic cylindrical surface using acoustic beamforming technique. In: In 4th Asia-Pacific Workshop on Structural Health Monitoring; Melbourne,Australia,December 5–7, 2012.

[14] D.H. Xiao, T. He, Q. Pan, et.al. A novel acoustic emission beamforming method with two uniform linear arrays on plate-like structures. Ultrasonics. 2014;54:737–745.

[15] J. Rose. Ultrasonic waves in solid media. Cambridge: Cambridge University Press; 1999.

[16] Young-Han Kim, Dae-Hyun Kim, Jung-Ho Han, Chun-Gon Kim. Damage assessment in layered composites using spectral analysis and Lamb wave. Composites: Part B. 2007;38:800–809.

[17] Friedrich Moser, Laurence J. Jacobs, Jianmin Qu. Modeling elastic wave propagation in waveguides with the finite element method. NDT & E International. 1999;32(4):225–234.

[18] Buli Xu,Victor Giurgiutiu. Single mode tuning effects on lamb wave time reversal with piezoelectric wafer active sensors for structural health monitoring. Journal of Nondestructive Evaluation. 2007;26:123–134.

http://dx.doi.org/10.5772/62413

[19] T.R.Hay, R.L.Royer, H.Gao, et al. A comparison of embedded sensor Lamb wave ultrasonic tomography approaches for material loss detection. Smart Materials and Structures. 2006;15:946–951.

[20] C. Zhou, Z.Q. Su, L.Cheng. Quantitative evaluation of orientation-specific damage using elastic waves and probability-based diagnostic imaging. Mechanical Systems and Signal Processing. 2011;25:2135–2156.

[21] H.K. Peng, G. Meng, F.C. Li. Modeling of wave propagation in plate structures using three-dimensional spectral element method for damage detection. Journal of Sound and Vibration. 2009;320:942–954.

[22] M.G. Silk, K.F. Bainton. The propagation in metal tubing of ultrasonic wave modes equivalent to Lamb waves. Ultrasonics. 1979;17:11–19.

IntechOpen